Chapter: 5

Control Operation of L_nC_{2n-2} Network Based MOHC for PV to Grid-Connected System

5.1. Introduction

So far, the working principles are covered: different operating modes, PWM scheme, leakage current mitigation, performance analysis, and a thorough comparison of the proposed converter with existing solutions. However, one crucial aspect that hasn't been discussed yet is the control operation of the proposed Multi-Output Hybrid Converter (MOHC).

Controlling the MOHC presents a unique challenge — primarily because it's designed to simultaneously manage both AC and DC loads. Ensuring smooth and stable operation for both types of outputs require a carefully designed and efficient control strategy.

This chapter focuses on the control methodology developed for the proposed converter. The converter is designed to operate in three distinct modes:

1. **Constant DC input with fixed AC and DC voltage output:** In this mode, the system maintains stable and fixed AC and DC voltage levels while drawing power from a constant DC input source.
2. **Constant DC input with fixed DC voltage and grid-connected AC voltage:** Here, the DC voltage remains regulated at a fixed level, while the AC output voltage synchronizes with and feeds power into the grid.
3. **PV input with fixed DC voltage and grid-connected AC voltage:** In this configuration, the converter takes input directly from a photovoltaic (PV) source. It maintains a stable DC voltage while ensuring the AC output remains grid-connected and synchronized.

Each of these operating modes is discussed in detail in the following sections of the chapter, and their performance has been validated through experimental results. These results demonstrate the effectiveness of the proposed control strategy and the versatility of the MOHC in handling various input and output conditions.

5.2. Transformation of AC Quantities to DC Quantities

Controlling DC quantities is generally more straightforward compared to AC quantities, mainly because DC values remain constant over time, while AC values vary sinusoidally. In the case of the Multi-Output Hybrid Converter (MOHC), which involves both DC and AC components, it becomes necessary to convert AC quantities into DC-like quantities to simplify the control strategy.

For the conversion of single-phase AC quantities into their DC equivalents, the process typically begins by sensing the AC voltage and current. These measured AC quantities are then transformed into the stationary α-β (alpha-beta) reference frame using the Clarke transformation. In this transformation, the α component represents the original in-phase quantity, while the β component is a 90-degree phase-shifted version of the α component as illustrated in Fig. 5.1. This transformation essentially projects the time-varying AC signals onto a two-axis coordinate system, simplifying their representation.

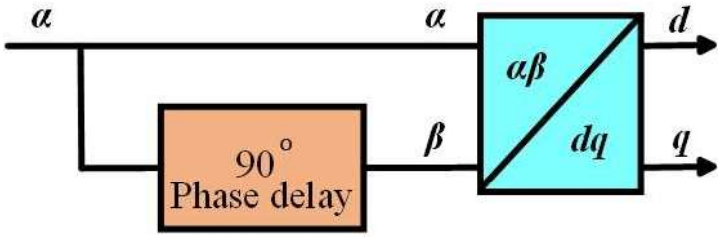

Fig. 5.1. Quadrature signal generation and αβ – dq transformation.

Once the α-β components are obtained, they are further converted into the rotating d-q (direct-quadrature) reference frame using the Park transformation. The d-axis (direct) component aligns with the rotating reference frame, capturing the real (in-phase) component of the AC signal, while the q-axis (quadrature) component captures the imaginary (90-degree out-of-phase) component. By using this rotating frame synchronized with the AC supply frequency, the transformed AC quantities appear as DC values, making them much easier to regulate and control. The stationary and rotating vector relationship representations are illustrated in Fig 5.2.

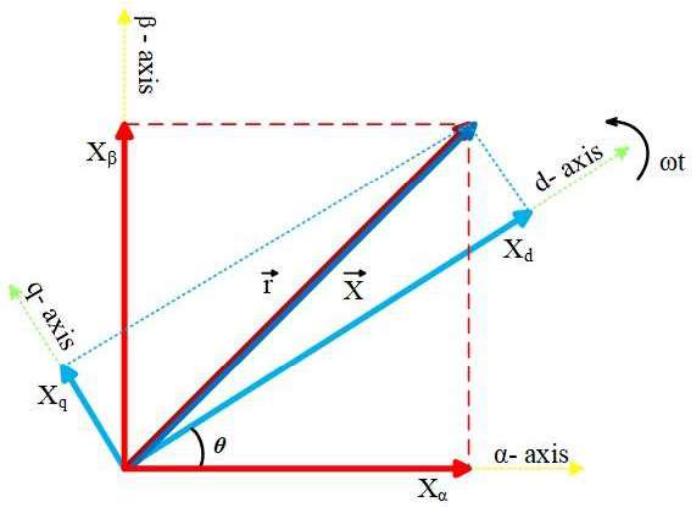

Fig. 5.2. The stationary and rotating vector relationship representations.

This systematic conversion from the time-varying AC quantities to steady-state DC-like quantities in the d-q frame is crucial for effective control of the MOHC. It simplifies the implementation of control algorithms, such as PI controllers, and enhances the dynamic response of the system.

5.3. Locked Loop (PLL)

A phase-locked loop (PLL) is an essential electronic system widely used to synchronize the phase and frequency of an incoming signal with a locally generated signal. PLLs are crucial in a variety of applications, including communication systems, power electronics, and grid synchronization, where maintaining precise timing and frequency alignment is vital.

A PLL typically consists of three core components: a phase detector, a loop filter, and a voltage-controlled oscillator (VCO), as illustrated in Fig. 5.3. Together, these components form a feedback loop that continuously adjusts the phase and frequency of the VCO output to match the incoming signal.

The process begins with the phase detector, which compares the phase of the input signal with the phase of the VCO output. The phase detector generates an error signal that reflects the difference between these two phases. This error signal is then passed through the loop filter, which smooths and conditions the signal by removing high-frequency noise and unwanted variations.

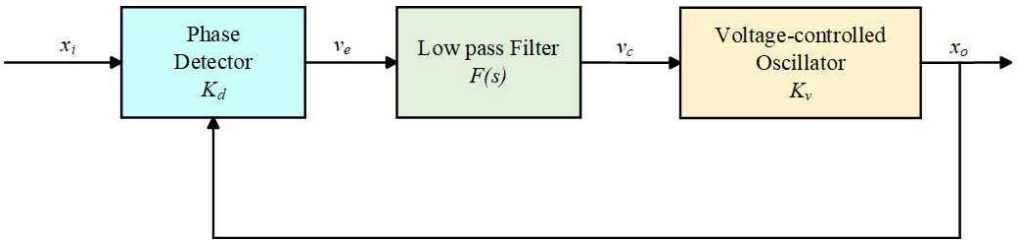

Fig. 5.3. Basic structure of phase locked loop (PLL).

The filtered signal is fed to the voltage-controlled oscillator, which adjusts its output frequency based on the input voltage it receives. As the feedback loop operates, the VCO continuously modifies its frequency and phase in a way that minimizes the phase difference between its own output and the incoming signal.

When the system reaches a state called "lock," the VCO frequency aligns perfectly with the average frequency of the input signal, and the phase difference between them becomes minimal or negligible. In this locked state, the PLL can accurately track any changes in the phase and frequency of the input signal, maintaining synchronization.

The ability of the PLL to achieve and maintain this locked condition is critical in ensuring stable and reliable operation in systems that require precise phase alignments, such as grid-connected inverters and communication networks.

Let x_i and x_o, be, respectively, the input and the VCO signals, which can be expressed as:

$$x_i(t) = A\cos(\omega_i t + \theta_i) \tag{5.1}$$

$$x_o(t) = A\cos(\omega_o t + \phi_o) \tag{5.2}$$

ω_i and ω_o are angular frequencies of the input signal and the VCO, θ_i and ϕ_o are their phase constants. The PD is a signal multiplier. If the loop is initially unlocked and the phase detector has a sinusoidal characteristic, the significant output signal $v_c(t)$ at the PD is given by:

$$v_c(t) = K_d\{\cos[(\omega_i - \omega_o)t + \theta_i - \phi_o] + \cos[(\omega_i + \omega_o)t + \theta_i + \phi_o]\} \tag{5.3}$$

where K_d is the gain of the PD. The higher frequency component with frequency $\omega_i + \omega_o$ is eliminated by LF, a low-pass filter. Therefore, the output of the LF is

$$v_c(t) = K_d\cos[(\omega_i - \omega_o)t + \theta_i - \phi_o] \tag{5.4}$$

After a period of time sufficiently long for transient, the VCO output signal x_o, becomes

synchronous with the input signal x_i. The signal x_o, can then be expressed as:

$$x_o(t) = B\sin[\omega_i t + \phi_o] \tag{5.5}$$

Comparison of equation 4.2 and 4.5 shows that the phase ϕo in 4.2 is a linear function of time given by:

$$\phi_o = (\omega_i - \omega_o)t + \phi_o \tag{5.6}$$

and the LF output signal $v_c(t)$ in (4) becomes a DC signal given by:

$$v_c(t) = K_d\cos(\theta_i - \phi_o) \tag{5.7}$$

The VCO is a frequency-modulated oscillator whose instantaneous angular frequency ω_{inst} is a linear function of the controlled signal vc(t), around the central angular frequency ω_o, i.e.,

$$\omega_{inst} = \frac{d(\omega_o t + \phi_o)}{dt} = \omega_o + K_v V_c(t) \tag{5.8}$$

and

$$\frac{d\phi_o}{dt} = K_v V_c(t) \tag{5.9}$$

where K_v is the VCO sensitivity from 5.6, 5.7 and 5.9

$$\omega_i - \omega_o = K_d K v\cos(\theta_i - \phi_o) \tag{5.10}$$

giving

$$\phi_o = \theta_i - \cos^{-1}\left(\frac{\omega_i - \omega_o}{K_d K_v}\right) \tag{5.11}$$

Substituting 5.11 into 5.7 yields

$$v_c = \frac{\omega_i - \omega_o}{K_v} \tag{5.12}$$

Eq. 5.12 clearly shows that it is the DC signal v_c, that changes the VCO frequency from its central value ω_o, to the input signal angular frequency ω_i, i.e.,

$$\omega_{inst} = \omega_o + K_v v_c = \omega_i \tag{5.13}$$

If the angular frequency difference $\omega_i - \omega_o$ is much lower than the product $K_d K_v$, 5.11 gives $\theta_i - \theta_o \approx \cos^{-1} = \pi/2$, indicating that the VCO signal is in phase quadrature with the input signal when the loop is in the lock. Strictly speaking, the phase quadrature corresponds to $\omega_i = \omega_o$. Thus, it is convenient to let

$$\theta_o = \phi_o + \frac{pi}{2} \tag{5.14}$$

Then 5.7 becomes

$$v_c(t) = K_d \sin(\theta_i - \theta_o) \tag{5.15}$$

The difference $\theta_i - \theta_o$ is the phase error between the two signals, which is null when the initial frequency offset is null. When the difference $\theta_i - \theta_o$, is sufficiently small, the following approximation is used:

$$v_c \approx K_d(\theta_i - \theta_o) \tag{5.15}$$

In view of 5.11, and 5.14 can be expressed as:

$$\phi_o = \theta_i - \cos^{-1}\left(\frac{\omega_i - \omega_o}{K_d K_v}\right) \tag{5.16}$$

The loop gain, denoted as $K = K_d \cdot K_v$, plays a crucial role in the sinusoidal-characteristic phase detector (PD). If the difference between ω_i and ω_o exceeds the loop gain K, as indicated by equation 5.17, it becomes impossible to find a suitable θ_o for maintaining the lock. Consequently, synchronization cannot be maintained, leading to the loss of lock in the loop.

5.4. Closed-Loop Operation

The closed-loop operation of the proposed converter plays a vital role in maintaining the desired output voltages, especially in a multi-output configuration where achieving independent control of each output voltage is a significant challenge. In this system, the outputs are governed by specific voltage equations, and the control variables — duty ratio (d) and modulation index (m_i) — are subject to a key constraint: $d + m_i \leq 1$. This interdependence of the outputs means they cannot be fully decoupled without a thoughtful control strategy.

The DC output voltage (V_{dc}) depends solely on the duty ratio (d), while the AC output voltage (V_{ac}) depends on both the duty ratio (d) and the modulation index (m_i). This relationship makes the control process intricate because any attempt to regulate V_{ac} by adjusting d also impacts V_{dc}. As a result, using d for controlling the AC voltage is avoided to prevent unwanted variations in the DC voltage.

To manage this complexity, the control strategy assigns the regulation of V_{dc} to the duty ratio (d) and the regulation of V_{ac} to the modulation index (m_i). This approach ensures

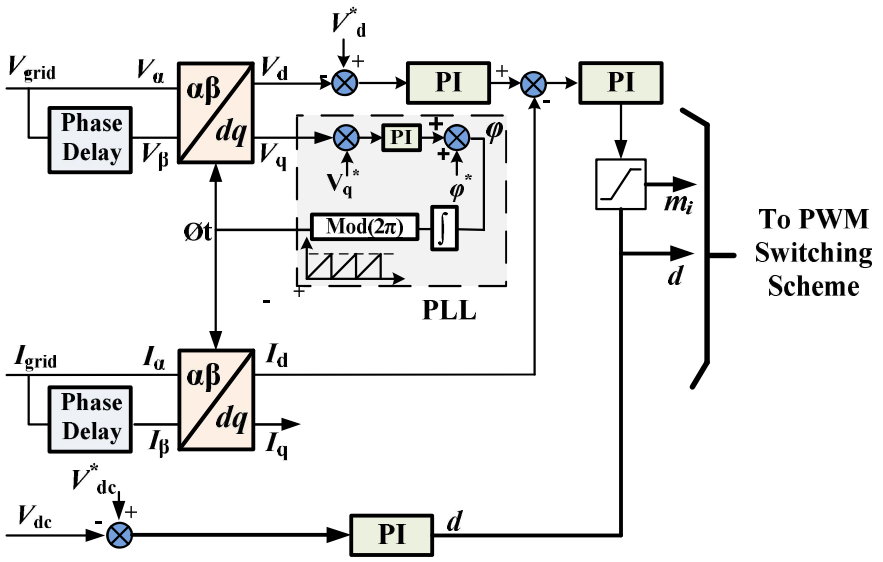

Fig. 5.4. Closed loop control logic.

that changes in one output voltage have minimal impact on the other, enabling more stable and independent control. Despite this, minor disturbances may still arise due to load variations, but these disturbances typically settle quickly.

The control scheme for the proposed converter is illustrated in Fig. 5.4. On the AC side, the load voltage (V_{ac}) and load current (I_{ac}) are sensed and transformed from the α-β frame to the dq frame using the α-β to dq transformation. This transformation converts sinusoidal quantities into DC-like quantities, simplifying the control process. The resulting V_d and I_d represent the peak amplitude of the AC voltage and current, respectively.

V_d is compared with the reference peak voltage (V_d^*), and the resulting voltage error is processed by a proportional-integral (PI) controller to generate the reference current (I_d^*). This reference current is then compared with the actual I_d, and the resulting error is fed into another PI controller to generate the modulation index (m_i). A phase-locked loop (PLL) is also employed, using the V_q component, to eliminate frequency errors and ensure synchronization of the AC section.

On the DC side, the DC voltage (V_{dc}) is directly compared with its reference value (V_{dc}^*). The voltage error is processed through a separate PI controller to generate the duty ratio (d). To maintain stability and prevent operational issues, a saturation block is introduced before mi to enforce the constraint $d + m_i \leq 1$.

The final outputs — duty ratio (d) and modulation index (m_i) — are then used to generate the pulse-width modulation (PWM) switching signals, as discussed in the previous chapters. This comprehensive control strategy ensures that both AC and DC outputs are independently regulated while maintaining overall system stability and performance.

5.5. Grid-Connected Operation of MOHC

The control structure of the proposed grid-connected converter, powered by a constant DC supply, is depicted in Fig. 5.5. This scheme ensures precise synchronization and efficient power transfer to the utility grid. At its core, the system begins by sensing the net grid current, I_{grid} along with the grid voltage, V_{grid}. These analog signals are converted into digital form by the ADC block integrated into TI's TMS320F28335 Delfino board, which features a 12-bit resolution for accurate signal acquisition.

Once digitized, the signals are fed into the quadrature signal generator (QSG), which derives the imaginary orthogonal component needed for transformation. The QSG output is then mapped into the synchronously rotating reference frame (dq frame) using the Park transformation. In this frame, the V_q component of the grid voltage is processed by the phase-locked loop (PLL). The PLL plays a crucial role in aligning the frequency and phase of the output voltage, V_{ac}, generated by the transformerless L_2C_2-HC converter with the grid voltage, V_{grid}, ensuring zero-phase disparity and proper

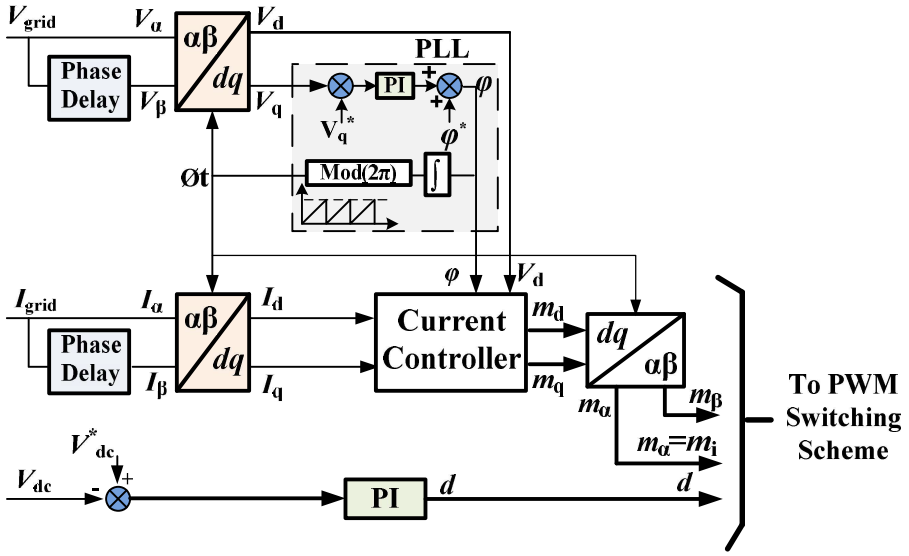

Fig. 5.5. Control logic for Grid-connected operations.

synchronization. Simultaneously, the direct (I_d) and quadrature (I_q) current components are sent to the current controllers for regulation.

To achieve a unity power factor and transfer high-quality AC power, the reference quadrature-axis current component I_q^* is set to zero. This ensures that the grid current, I_{grid}, remains perfectly in phase with the grid voltage, V_{grid}. The current controllers generate modulation indices (m_d and m_q), which are transformed back into the stationary reference frame (αβ) using the inverse Park transformation. This yields the m_α signal aligned with the grid voltage phase. The signal is scaled by the DC-link voltage, V_{dc}, producing the reference signal, m_i, which is subsequently fed into the pulse-width modulation (PWM) switching scheme.

The duty cycle of the PWM block remains constant when the power supplied to the grid is drawn from the stable DC source. However, the duty cycle can also be dynamically adjusted based on the comparison between the reference DC voltage and the output DC voltage. This voltage error is processed through a proportional-integral (PI) controller, ensuring steady-state performance and minimizing deviations. The PWM block uses the calculated modulation index to generate precise gate signals, which drive the proposed converter's switches and facilitate the controlled injection of current into the utility grid.

The entire control strategy is executed using the TI's TMS320F28335 Delfino board, renowned for its real-time processing capabilities and high-resolution ADC. By maintaining synchronization between the grid voltage, V_{grid}, and the output voltage, V_{ac}, and ensuring that V_{ac}'s peak voltage slightly exceeds or matches V_{grid}, the converter remains optimally activated, consistently delivering the intended current into the grid with high efficiency and power quality.

5.6. MPPT and Grid-Connected Operation of MOHC

Harnessing the full potential of a PV panel — by efficiently supplying DC power and feeding AC power into the grid — is a complex and challenging process. The L_2C_2-HC control system plays a crucial role in managing this, and its operation can be broadly divided into two key functions. First, it maximizes the efficiency of the solar panel through Maximum Power Point Tracking (MPPT), ensuring the panel consistently delivers its highest possible output. Second, it ensures smooth and reliable integration

with the AC grid, maintaining stability and synchrony between the solar power system and the grid infrastructure. Together, these functions enable the system to fully capitalize on solar energy while contributing clean power to the grid.

5.6.1. MPPT Operation

The proposed Multi-Output Hybrid Converter (MOHC) is designed to simultaneously supply both AC and DC loads from a single PV input, making the most of the available solar power. First, the system prioritizes the DC load's power requirements to ensure the immediate demand is met. Once the DC load is satisfied, any surplus power from the PV panel is directed to the AC grid using a Maximum Power Point Tracking (MPPT) algorithm, maximizing the panel's efficiency. This ensures that no available solar power goes to waste — any excess energy beyond the DC load's needs is seamlessly fed into the grid for optimal utilization of the PV panel's capacity. This relationship is expressed by the equation:

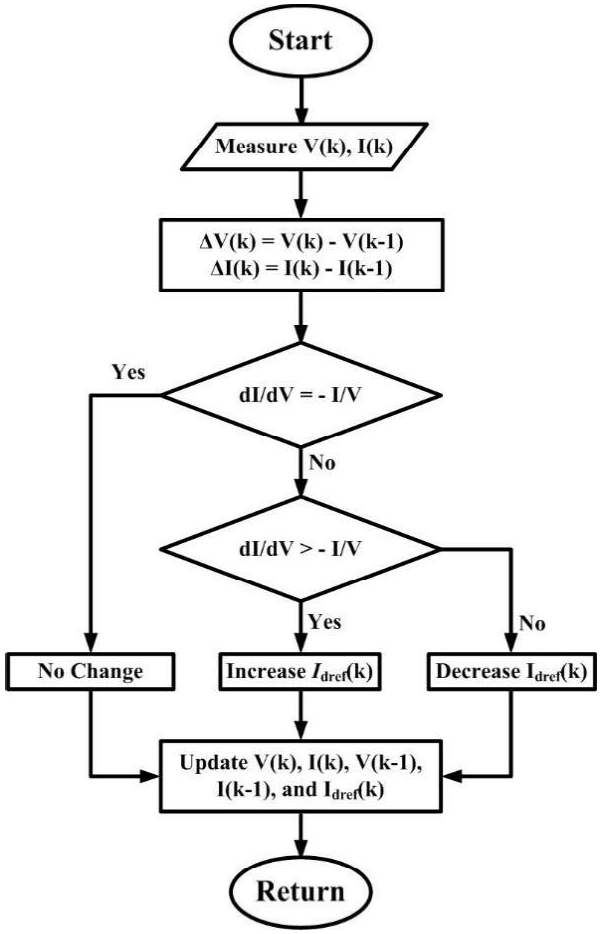

Fig. 5.6. Incremental conductance flowchart for proposed MOHC.

$$P_{MPP} - P_{dc} = P_g \tag{5.17}$$

where P_{MPP} is the maximum power output of the PV panel, P_{dc} is the power supplied to the DC load, and P_g is the power injected into the AC grid.

The system uses the Incremental Conductance (INC) method for MPPT, as shown in Fig. 5.6. INC is a widely used approach for optimizing the power output of PV systems, ensuring they operate at their Maximum Power Point (MPP) even as environmental conditions change. By selecting different parameters for increment or decrement, the INC method can adapt to different operational cases, always driving the PV array toward its peak efficiency.

In this method, the PV array voltage (V_{PV}) is typically the key parameter adjusted to achieve the MPP. The reference current (I_{dref}) is generated by the MPPT algorithm to control the d-axis current (I_d), which is responsible for injecting real power into the grid. By continuously adjusting I_{dref}, the algorithm ensures that the product of the PV voltage (V_{PV}) and PV current (I_{PV}) — representing the total PV power (P_{PV}) — aligns with the panel's maximum power output (P_{MPP}). When this balance is achieved, the system operates at its optimal power point, fully harnessing the PV array's potential.

5.6.2. MPPT with Grid Connected Operation

Fig. 5.6 provides a comprehensive overview of the grid-connected operation of the proposed system. The control strategy begins with the detection of key grid parameters:

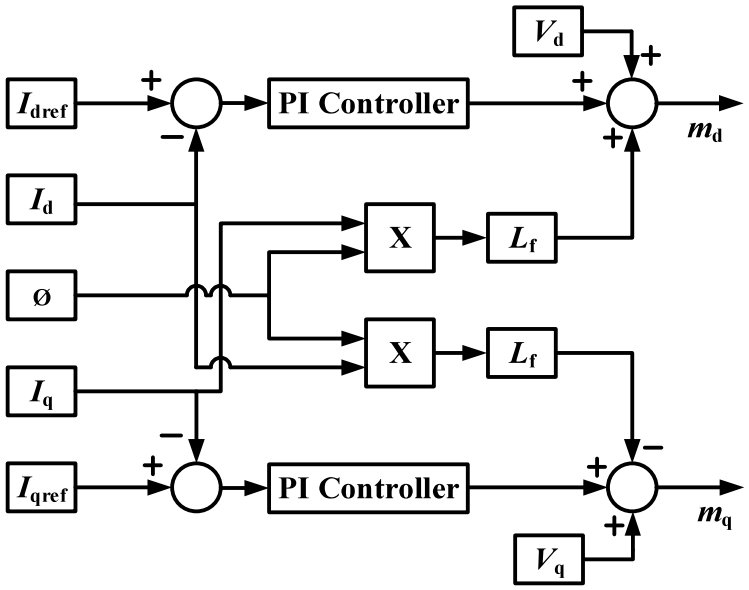

Fig. 5.7. Control strategy of proposed MOHC.

the grid voltage (V_{grid}) and the grid current (I_{grid}). These signals are carefully measured and then passed through 90^0-degree phase shifters, which facilitate their transformation into the stationary α-β reference frame. Once in this frame, the α-β current components are converted into the synchronous reference frame (dq domain), producing the direct and quadrature components: I_d, I_q, V_d, and V_q.

A crucial part of this process is the Phase-Locked Loop (PLL) module, which serves two primary functions. First, it synchronizes the frequency and phase of the output voltage (V_{ac}) produced by the proposed L_2C_2-HC converter with the grid voltage. Second, it ensures there is no phase difference between the grid voltage (V_{grid}) and the output voltage (V_{ac}). This alignment is essential for efficient and stable grid-connected operation.

The dq components (I_d, I_q, V_d) and the system's angular frequency (Ø), along with the reference current (I_{dref}) generated by the Maximum Power Point Tracking (MPPT) system, are then fed into the current controller. This controller plays a vital role in regulating the current injected into the grid, which directly determines the amount of power delivered to the AC grid.

For the DC voltage control, the system maintains a reference DC voltage (V_{dc}^*) of 230 V. This reference voltage is continuously compared with the actual sensed DC output voltage. The difference between the two is processed by a Proportional-Integral (PI) controller, which adjusts the duty ratio (d) to stabilize the DC voltage at the output port.

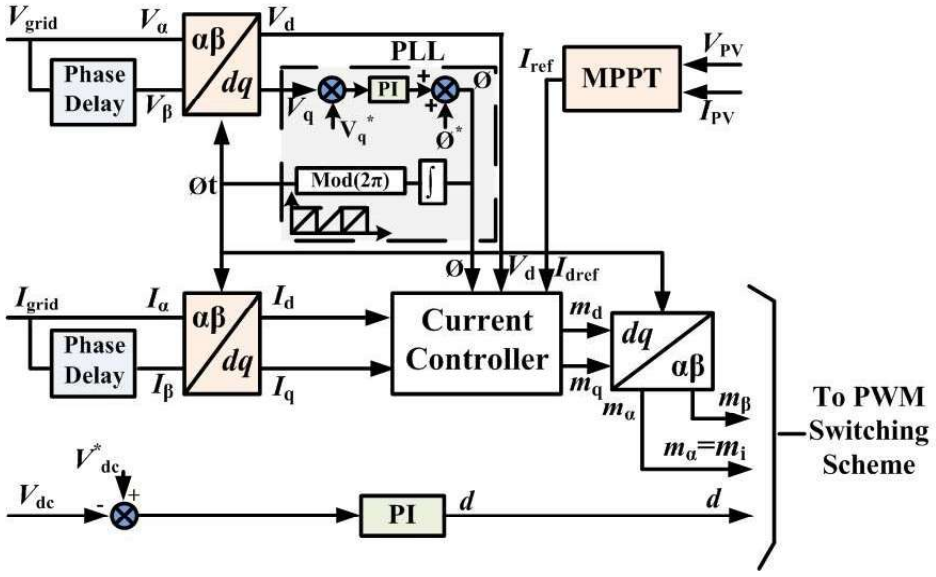

Fig. 5.6. Control operation of proposed MOHC for PV to Grid operation.

When it comes to controlling the AC quantities, the system converts them into DC quantities in the dq domain. The d-axis component of the grid current (I_d) represents the real power injected into the grid, while the q-axis component (I_q) corresponds to the reactive power. By managing I_d and I_q, the system can control the real and reactive power delivered to the grid.

After determining the dq voltage and current components, the current controller executes the control strategy as illustrated in Fig. 5.7 using the following equations (5.18) and (5.19):

$$m_d = \left(I_{dref} - I_d\right)PI + V_d + I_q L_f Ø \tag{5.18}$$

$$m_q = \left(I_{qref} - I_q\right)PI + V_q - I_d L_f Ø \tag{5.19}$$

Here, m_d and m_q are the intermediate control signals, which are then transformed back into the stationary α-β frame through the inverse park transformation. This yields m_α and m_β, where m_α acts as the modulation index and serves as the modulating wave.

Finally, the modulation index is used by the Pulse Width Modulation (PWM) block to generate gate signals. These gate signals drive the proposed converter, ensuring the desired current is injected into the utility grid while achieving maximum power point performance (P_{MPP}). The entire control strategy is implemented using Texas Instruments' TMS320F28335 Delfino microcontroller board, which was discussed in detail in the previous chapters.

5.7. Experimental Verification

The control strategy of the proposed converter has been thoroughly discussed for various operating conditions, including dynamic scenarios, grid-connected operation, and PV-to-grid power transfer. To validate the effectiveness of the proposed approach, experimental results have been presented for each of these conditions.

5.7.1. Dynamic Variation under Constant DC Input with Fixed AC and DC Voltage Output

The dynamic behaviour of the proposed converter under varying load and input conditions is illustrated in Fig. 5.9. The response to DC load variations is shown in Fig. 5.9(a) and Fig. 5.9(b). In Fig. 5.9(a), a sudden decrease in DC load current from 3A to 2.4A is observed, while Fig. 5.9(b) captures a sharp increase from 2.4A to 3.6A. In both

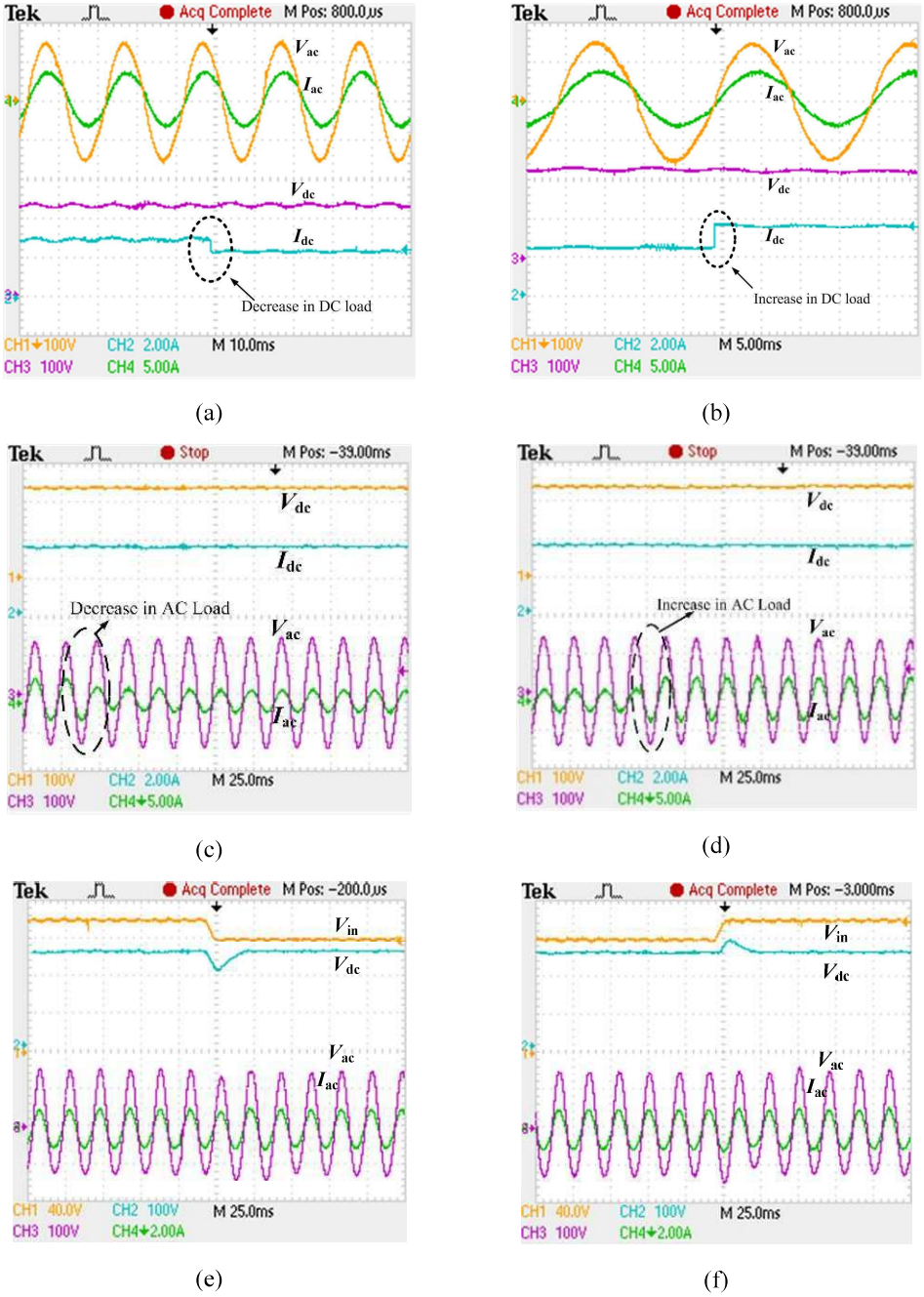

Fig. 5.9. Dynamic performance of converter (a) When DC load is decreased. (b) Load is increased. (c) When the AC load is decreased. (d) AC load is increased. (e) When the Input voltage is decreased. (f) Input voltage is increased.

cases, the DC and AC voltage remain largely unaffected, demonstrating the system's stability.

Similarly, the impact of AC load variations is depicted in Fig. 5.9(c) and Fig. 5.9(d). Fig. 5.9(c) shows a sudden drop in AC load current from 3.5A to 2.1A, while Fig. 5.9(d)

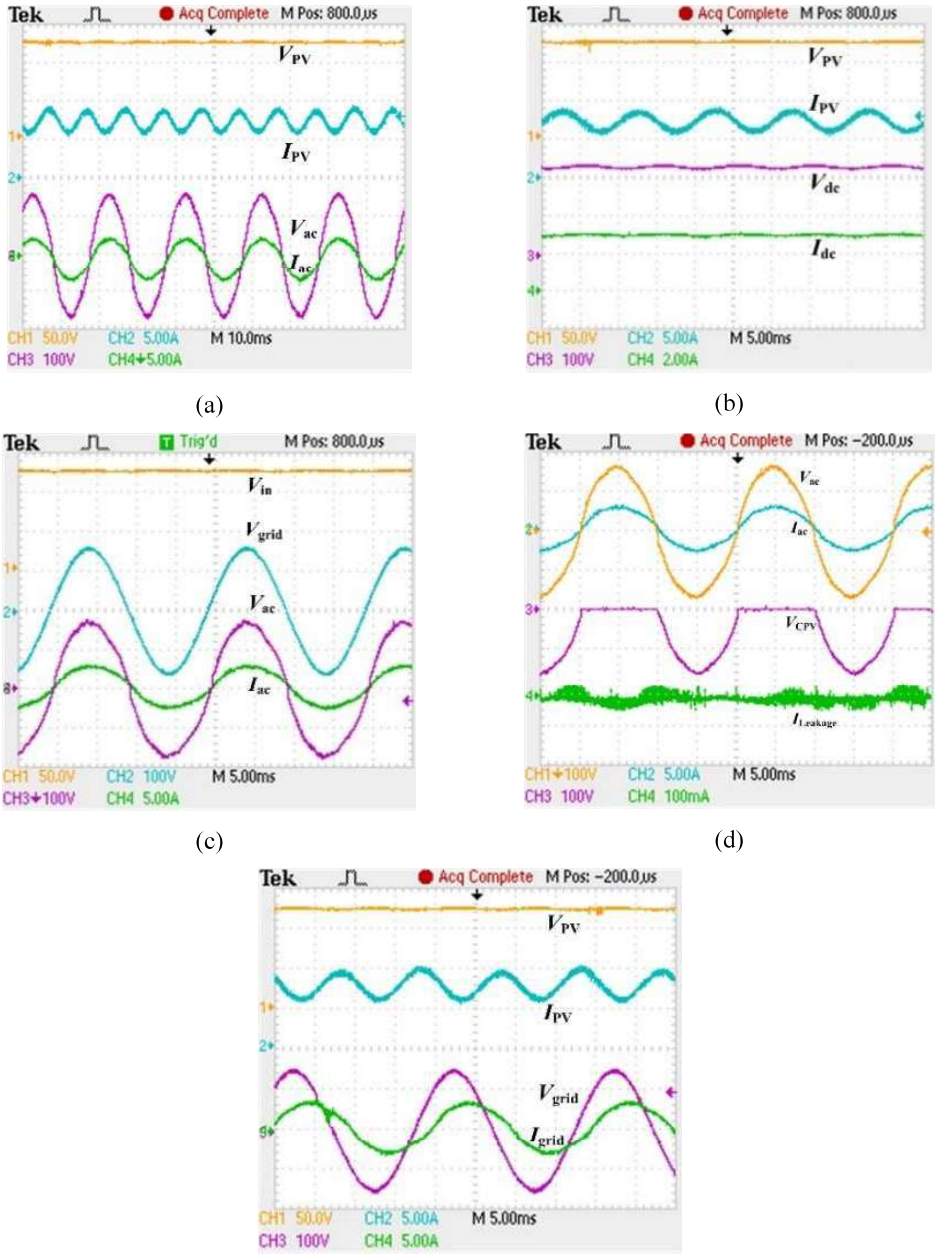

Fig. 5.10. Grid Connected operation of L_2C_2-HC (a) AC voltage and current with respect to the input PV voltage and current. (b) DC voltage and current with respect to the input PV voltage and current. (c) AC voltage and current with the PV input and grid voltage. (d) Leakage current profile. (e) Reactive power injected to the grid.

illustrates a swift rise from 2.1A to 3.5A — both scenarios again reflect minimal influence on DC and AC voltage.

The converter's response to dynamic input voltage changes is presented in Fig. 5.9(e) and Fig. 5.9(f). Fig. 5.9(e) shows the system's performance when the input voltage

drops from 140V to 120V, and Fig. 5.9(f) captures its behavior when the voltage increases from 120V to 140V. Despite these fluctuations, the DC and AC voltage remain stable, highlighting the converter's robustness and reliability in maintaining consistent output.

5.7.2. Grid-Connected Operation of MOHC

Figure 5.10 presents the experimental results obtained under grid-connected conditions, which are discussed in detail below.

In Fig. 5.10(a), the converter's input voltage and current are shown as 120V and 8A, respectively. Alongside, the AC output voltage of 115V and an AC current of 2A are depicted, highlighting the converter's stable performance in supplying AC power.

Fig. 5.10(b) illustrates the DC output characteristics, showing a steady DC voltage of 230V and a DC current of 3A, confirming the converter's ability to maintain consistent DC power output.

The synchronization between the converter and the grid is demonstrated in Fig. 5.10(c), where the grid voltage of 110V is shown to be perfectly in phase with the converter's output voltage. The figure also displays the grid current being injected into the grid, emphasizing proper grid integration and power quality.

The safety performance of the system is validated in Fig. 5.10(d), which presents the leakage current profile. The leakage current, scaled at 100mA, is observed to remain well within the permissible safety limits, ensuring compliance with standard regulations.

Finally, Fig. 5.10(e) shows the injection of 2A of reactive current into the grid, operating with a power factor of 0.8 lagging. This demonstrates the converter's capability to support reactive power compensation and improve grid stability.

5.7.3. MPPT to Grid-Connected Operation

As discussed earlier, achieving Maximum Power Point Tracking (MPPT) in the proposed Multi-Output Hybrid Converter (MOHC) during grid-connected operation is a challenging task. This is because the converter must simultaneously manage power extraction from the PV panel, meet the demands of the DC load, and efficiently transfer

any surplus power to the grid. The complete setup of the proposed setup has been illustrated in Fig. 5.11.

In the initial stage, the converter extracts power from the PV panel and prioritizes supplying the required energy to the DC load. Once the DC load demand is met, any excess power generated by the PV panel is fed into the grid, ensuring optimal utilization of the available solar energy.

To validate this operational strategy, experimental results demonstrating the converter's performance under these conditions are presented below.

- **MPPT Characteristics of the Proposed MOHC**

Fig. 5.12(a) illustrates the dynamic behavior of key parameters — PV voltage (V_{PV}), PV current (I_{PV}), AC voltage (V_{ac}), and grid current (I_{grid}) — at the moment when Maximum Power Point Tracking (MPPT) is initiated. A notable observation here is the swift and efficient tracking of the Maximum Power Point (MPP), demonstrating the system's fast response and effective control strategy.

Complementing this, Fig. 5.12(b) presents the variation in the equivalent resistance (R_{eq}) as the converter locks onto the Peak Maximum Power Point (P_{MPP}) under an irradiance level of 1000 W/m². The data for this plot was meticulously gathered through experimental measurements using the Chroma 621000H-600S Soft Panel, ensuring high accuracy and reliability in capturing the converter's real-time performance. Together, these figures validate the system's capability to quickly and reliably achieve

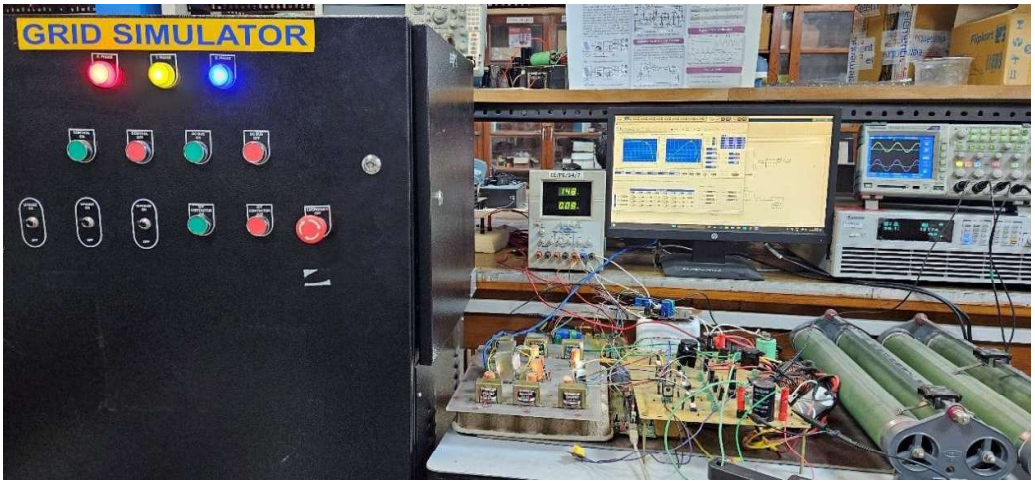

Fig. 5.11. Complete experimental setup for PV to Grid tied MOHC.

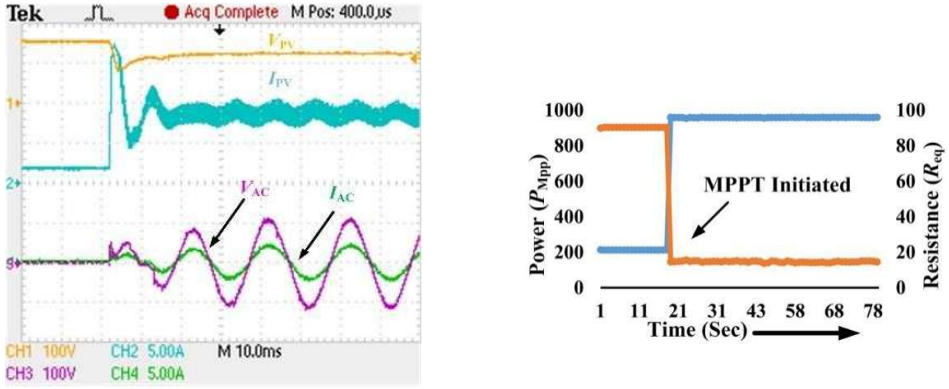

(a) (b)

Fig. 5.12. MPPT Characteristics (a) Initiation of MPPT (b) Variation in Req with the variation in power.

MPPT while maintaining stable grid-connected operation, highlighting the converter's robustness in practical deployment scenarios.

➢ Dynamic MPPT Transient During Irradiance Variation

Fig. 5.13(a) and Fig. 5.13(b) illustrate the dynamic response of key system parameters — PV voltage (V_{PV}), PV current (I_{PV}), AC voltage (V_{ac}), and grid current (I_{grid}) — to

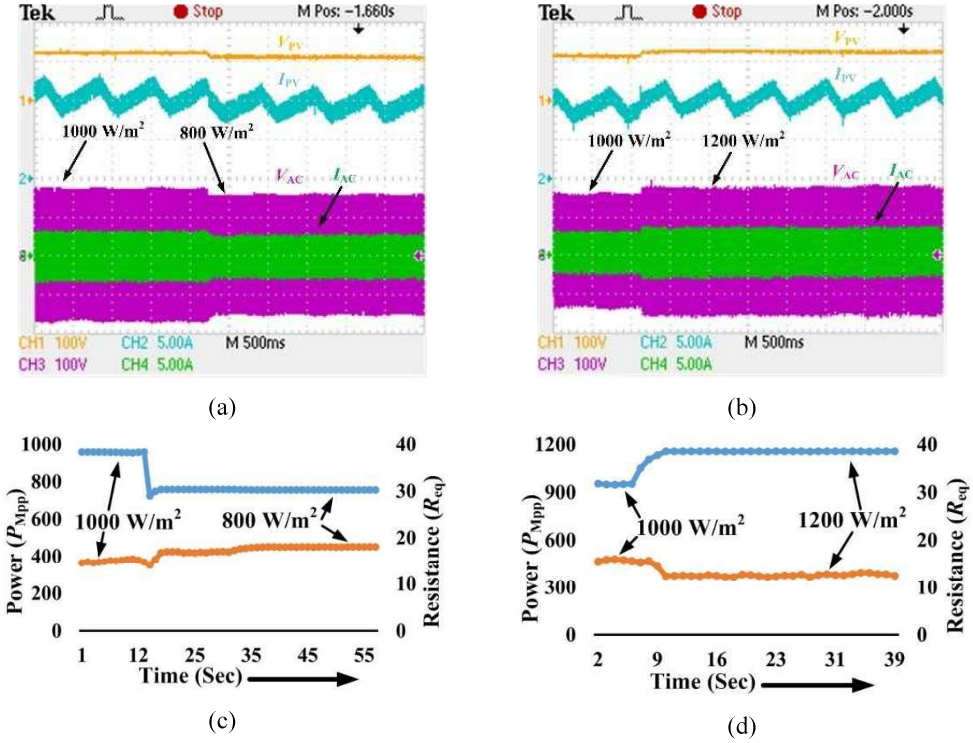

(a) (b)

(c) (d)

Fig. 5.12. MPPT Dynamics (a) Irradiance decreases. (b) Irradiance decreases (c) Variation in R_{eq} for change decrease in Irradiance. (d) Variation in R_{eq} concerning increase in Irradiance.

variations in solar irradiance. Specifically, Fig. 5.13(a) captures the system's behaviour when irradiance drops from 1000 W/m² to 800 W/m², while Fig. 5.13(b) shows the response when irradiance increases from 1000 W/m² to 1200 W/m². In both cases, the converter maintains stable performance, quickly adapting to changing conditions without any noticeable disruption in AC voltage or grid current.

Complementing these observations, Fig. 5.13(c) and Fig. 5.13(d) present the variation in power output and the equivalent resistance (R_{eq}) corresponding to the irradiance changes depicted in Fig. 5.13(a) and Fig. 5.13(b). Fig. 5.13(c) shows the system's response to the drop in irradiance from 1000 W/m² to 800 W/m², while Fig. 5.13(d) captures the impact of the rise from 1000 W/m² to 1200 W/m². These results clearly demonstrate the converter's ability to track the Maximum Power Point (MPP) efficiently, adjusting power output and R_{eq} with high accuracy.

Observing the overall behaviour from Fig. 5.13(a) through Fig. 5.13(d), it becomes evident that fluctuations in irradiance have no adverse effect on the proposed MOHC's performance during grid-connected operation. The system remains stable and reliable, ensuring consistent power delivery to both DC loads and the grid, even under rapidly changing solar conditions.

- **Dynamic Transient During Load Change Operation**

A sudden decrease in the DC load causes an immediate rise in the AC current injected into the grid, as depicted in Fig. 5.13(a). This behaviour occurs because the reduction in DC load demand leaves more surplus power available from the PV system, which is then redirected to the grid. This adjustment is crucial to ensure that the PV system

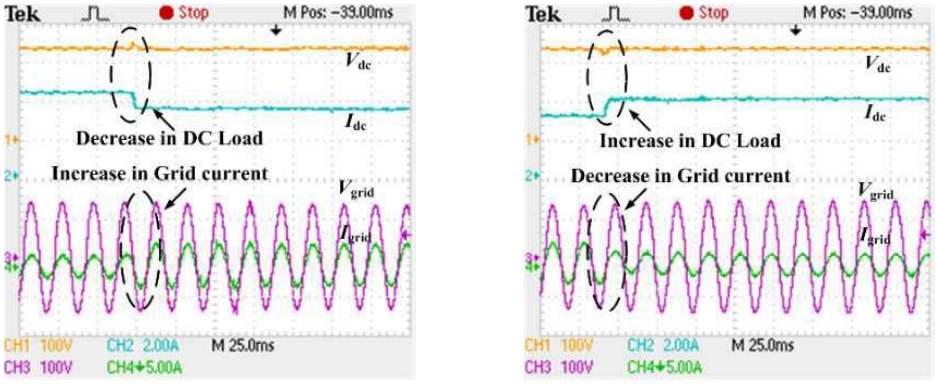

(a) (b)

Fig. 5.14: Dynamic Load change (a) Decrease in DC load. (b) Increase in DC Load.

continues operating at its Maximum Power Point (MPP), optimizing energy extraction and grid contribution.

On the other hand, Fig. 5.13(b) illustrates the opposite scenario — when the DC load demand suddenly increases, the AC current injected into the grid decreases. In this case, more of the available PV power is diverted to meet the higher DC load requirement, resulting in less excess power available for grid injection. Despite these variations, the system consistently prioritizes maintaining the MPP of the PV system, ensuring efficient and stable power management across both DC loads and grid-connected operations.

5.8. Summary

In this chapter, the control operation of the proposed Multi-Output Hybrid Converter (MOHC) has been discussed in detail. The unique challenge of the MOHC lies in its ability to simultaneously cater to both DC and AC loads, which makes its operation more complex compared to conventional power converters. To address this, the converter has been analyzed under three distinct operating conditions, and the proposed control algorithm for each condition has been thoroughly explained.

One of the most challenging aspects of this system is the integration of the PV system with the grid. This chapter introduces and discusses the control strategy specifically designed for PV-to-grid operation, ensuring efficient power transfer and maintaining Maximum Power Point Tracking (MPPT) while balancing DC load requirements and grid injection. The effectiveness of the proposed algorithms has been validated through experimental results, demonstrating the system's robustness and reliability under various dynamic conditions.

The L_nC_{2n-2} network has been extensively explored as a single-stage system, and its potential for use in the Multi-Output Hybrid Converter (MOHC) for simultaneous AC and DC supply has been thoroughly validated—both conceptually and through experimental results. This validation has demonstrated the network's promising performance and versatility.

Despite its impressive capabilities in single-stage applications, the L_nC_{2n-2} network also shows great promise for two-stage and isolated systems. In a conventional two-stage power electronic system, an intermediate DC link is often used, where a high-value,

large-sized electrolytic capacitor plays a crucial role in stabilizing voltage. However, this component is widely regarded as the weakest link in the system due to its limited lifespan and high susceptibility to failure. This makes the reliability of the entire setup heavily dependent on a single, failure-prone element.

To address this critical issue, the electrolytic capacitor in the DC link is replaced with more robust film capacitors. Film capacitors offer several significant advantages: they provide higher current density, are more compact, and deliver smoother, ripple-free voltage operation. This substitution not only enhances the system's reliability but also extends its overall operational lifespan.

Building on these improvements, a novel topology of the L_nC_{2n-2} network-based isolated resonant converter has been proposed. This advanced design eliminates the need for electrolytic capacitors entirely, using film capacitors instead. By removing the most failure-prone component, this innovation ensures a far more durable and dependable system.

One of the key strengths of resonant converters lies in their high efficiency and soft-switching capabilities, which make them ideal for DC-DC conversion. However, they often face challenges in maintaining smooth voltage regulation, as voltage gain is typically dependent on the transformer turns ratio—making them less suitable for applications with wide input voltage variations.

The integration of L_nC_{2n-2} network with the resonant converter addresses this limitation by enabling smooth voltage gain control through a single switch, adjusted by varying its duty cycle. This unique feature allows the system to handle wide input voltage variations efficiently, ensuring consistent and stable output.

The following chapter provides a detailed analysis and in-depth discussion of this enhanced system, highlighting its improved performance and superior reliability.